Single polymer dynamics under large amplitude oscillatory extension

Yuecheng Zhou[1] and Charles M. Schroeder[1,2,3,*]

[1]*Department of Materials Science and Engineering, University of Illinois at Urbana-Champaign, Urbana, Illinois 61801, USA*

[2]*Department of Chemical and Biomolecular Engineering, University of Illinois at Urbana-Champaign, Urbana, Illinois 61801, USA*

[3]*Center for Biophysics and Quantitative Biology, University of Illinois at Urbana-Champaign, Urbana, Illinois 61801, USA*

(Received 29 March 2016; published 20 September 2016)

Understanding the conformational dynamics of polymers in time-dependent flows is of key importance for controlling materials properties during processing. Despite this importance, however, it has been challenging to study polymer dynamics in controlled time-dependent or oscillatory extensional flows. In this work, we study the dynamics of single polymers in large-amplitude oscillatory extension (LAOE) using a combination of experiments and Brownian dynamics (BD) simulations. Two-dimensional LAOE flow is generated using a feedback-controlled stagnation point device known as the Stokes trap, thereby generating an oscillatory planar extensional flow with alternating principal axes of extension and compression. Our results show that polymers experience periodic cycles of compression, reorientation, and extension in LAOE, and dynamics are generally governed by a dimensionless flow strength (Weissenberg number Wi) and dimensionless frequency (Deborah number De). Single molecule experiments are compared to BD simulations with and without intramolecular hydrodynamic interactions (HI) and excluded volume (EV) interactions, and good agreement is obtained across a range of parameters. Moreover, transient bulk stress in LAOE is determined from simulations using the Kramers relation, which reveals interesting and unique rheological signatures for this time-dependent flow. We further construct a series of single polymer stretch-flow rate curves (defined as single molecule Lissajous curves) as a function of Wi and De, and we observe qualitatively different dynamic signatures (butterfly, bow tie, arch, and line shapes) across the two-dimensional Pipkin space defined by Wi and De. Finally, polymer dynamics spanning from the linear to nonlinear response regimes are interpreted in the context of accumulated fluid strain in LAOE.

DOI: 10.1103/PhysRevFluids.1.053301

I. INTRODUCTION

The processing of complex fluids and soft materials often involves highly nonequilibrium states that cannot be understood in terms of equilibrium principles or thermodynamics [1]. From this view, it is essential to understand the rheological behavior of complex fluids in order to control materials properties during flow-based processing. To address this issue, the dynamic behavior of polymer solutions and melts is commonly studied using a set of canonical rheological tests based on shear flow or extensional flow [1]. Simple shear flow consists of equal amounts of fluid rotation and compression-extension [2], thereby resulting in interesting albeit complex dynamics at the microscale [3]. Shear flow is a ubiquitous flow, generated any time a fluid moves past a solid stationary boundary, and hence can be implemented using rotational cone and plate or parallel-plate rheometers. For these reasons, bulk shear rheometry has evolved into a universal method used to probe the dynamics of polymeric materials, including both transient and steady-state shear rate experiments and controlled stress or step-strain experiments [1].

*cms@illinois.edu

Small-amplitude oscillatory shear (SAOS) has been used as a common method to probe the response of complex fluids in the limit of small deformations. However, SAOS probes only the linear viscoelastic properties of materials [4,5], which is usually insufficient to fully understand the nonlinear properties of fluids with complex micro- or nanostructures. To address this issue, large-amplitude oscillatory shear (LAOS) was developed [6,7] and widely adopted in recent years to characterize the nonlinear rheological behavior of complex fluids [8,9]. In LAOS, the nonlinear stress response of complex fluids is no longer a simple first-order sinusoidal function; rather, it typically appears as a complex distorted shape with higher order harmonics that depend on the material structure. Mathematical models have been developed to analyze these unique nonlinear stress responses [10–12], based on which complex fluids can be identified [11,13].

Extensional flow is considered to be a strong flow that can induce high levels of microstructure deformation. Unlike simple shear, extensional flow contains no elements of fluid rotation and consists only of extensional-compressional character [2]. For these reasons, extensional flow and rheological tests based on extension-dominated flows are generally more difficult to experimentally implement. To this end, development of the filament stretching rheometer (FISER) and the capillary breakup extensional rheometer (CABER) has enabled bulk extensional rheology measurements on complex fluids, thereby revealing the response of materials to strong extensional flows [14,15]. Although the vast amount of bulk extensional rheometry focuses on transient step strain or step strain-rate experiments, a few prior studies have reported time-dependent extensional flow measurements using bulk rheometry [16–18]. Using a customized FISER instrument, Rasmussen *et al.* [16] and Bejenariu *et al.* [17] examined the soft elasticity of low-dispersity polystyrene (PS) melt and polydimethylsiloxane (PDMS) networks through large-amplitude oscillatory extension (LAOE). A unique periodic response for the elongational stress was found, but both experiments were limited by relatively small varying elongational strain rates.

In recent years, single molecule techniques have been used to probe the dynamics of soft materials at the molecular scale [19,20]. Single polymer methods allow for the direct observation of polymer-chain dynamics under nonequilibrium conditions, which serves as a useful complement to bulk-level rheological measurements that characterize ensembles of polymer chains. Prior work has focused on steady and transient polymer dynamics in shear flow [21–26], planar extensional flow [27–30], and linear mixed flows [31,32], thereby revealing valuable information on dynamic behavior such as molecular individualism [33]. In nearly all cases, however, the vast majority of single polymer studies has employed simple on-off step functions for imposing so-called flow forcing functions for both transient and steady-state experiments. From this perspective, there is a general need to study single polymer dynamics in more complicated, time-dependent transient flows, and these experiments would serve as a direct analogy to macroscopic oscillatory rheological measurements.

In this work, we study the dynamics of single polymers in large amplitude oscillatory extension (LAOE) using a combination of experiments and Brownian dynamics (BD) simulations. LAOE experiments are facilitated by the Stokes trap [34], which is a new method for multiplexed trapping and controlled manipulation of objects in extensional flows. We find that polymers experience periodic cycles of compression, re-orientation, and extension in LAOE, with single chain dynamics controlled by the dimensionless flow strength Weissenberg number (Wi) and probing frequency Deborah number (De). Experimental results are compared to BD simulations with and without intramolecular hydrodynamic interactions (HI) and excluded volume (EV) interactions, and we observe that BD simulations accurately capture the dynamics of single polymers in LAOE over a wide range of control parameters. The polymer contribution to the bulk stress is also computed through the Kramers expression, which shows interesting rheological behavior for polymers in LAOE. Moreover, we determine a series of single polymer stretch-flow rate curves (defined as single molecule Lissajous curves) as a function of Wi and De. Qualitatively different dynamical signatures of the single molecule Lissajous curves are observed across the two-dimensional Pipkin space defined by Wi and De, and several of these shapes are verified by experiments. Finally, polymer dynamics from the linear to nonlinear response regimes across Pipkin space are quantitatively analyzed in the context of accumulated fluid strain in LAOE. Taken together, our results provide direct observation

of polymer chain microstructure during time-dependent and oscillatory dynamics in LAOE, which will be useful for interpreting bulk rheological data in time-dependent flows.

II. EXPERIMENTAL METHODS: LARGE-AMPLITUDE OSCILLATORY EXTENSION

A major challenge in studying single polymer dynamics in LAOE is the ability to generate precisely controlled flow fields while simultaneously confining single chains in the vicinity of a stagnation point in planar extensional flow. Fluid elements separate exponentially in time in extensional flows, and slight perturbations or translational fluctuations of a particle away from the fluid stagnation point will result in the object of interest being rapidly convected away from the image area. In order to generate controlled LAOE flows while simulataneously confining single polymers for long times, we used the Stokes trap [34], which relies on model predictive control (MPC) to precisely position and manipulate single or multiple particles in flow. Briefly, the center-of-mass position of a target polymer is determined in real time using fluorescence imaging and image analysis (LABVIEW), and this information is communicated to the MPC feedback controller. Next, the controller determines the flow rates required to confine the polymer chain at the target position and at the desired flow rate, and these updates are implemented using computer-controlled pressure regulators. The controller response time is $\approx$500 μs, and the total time for one control cycle loop is $\approx$30 ms; these time scales are much shorter than the LAOE cycle times T in this work, which allows for high-precision control over both the polymer position and the time-dependent LAOE flow rates. Additional details on the Stokes trap can be found in prior work [34].

In the context of LAOE, the Stokes trap is implemented using a four-channel cross-slot microfludic device (Fig. 1), wherein opposing channels serve as alternating directions of compression-rotation, thereby enabling single DNA molecules to be trapped and manipulated in precisely controlled LAOE flows. Fluid flow is driven by pressurized inlets connected to four computer-controlled pressure regulators (Proportion-Air Inc.). The LAOE experiment is performed by alternating the positive pressures in the top-bottom and left-right channels in a sinusoidal manner (Fig. 1). During the first half of the sinusoidal strain rate input ($0 < t < T/2$), fluid is pumped into the flow cell from ports $p1$ and $p3$ such that the y axis is the extensional axis and the x axis is the compressional axis. During the second half of the cycle ($T/2 < t < T$), fluid is pumped into the flow cell from ports $p2$ and $p4$ such that the y axis is the compressional axis and the x axis is the extensional axis. During this process, single DNA molecules are trapped near the stagnation point using a feedback controller [34] that applies small pressures to the opposing ports. The feedback control pressures δ are negligible compared to the primary pressure P used to generate the oscillatory extensional flow, such that $\delta \ll P$ for the majority of the cycle. Using this approach, a sinusoidal oscillatory planar extensional flow is applied in the cross-slot device, and the local fluid velocity in the vicinity of the stagnation point is described by

$$\mathbf{v} = (v_x, v_y, v_z) = [\dot{\epsilon}_x(t)x, \dot{\epsilon}_y(t)y, 0] = \left[-\dot{\epsilon}_0 \sin\left(\frac{2\pi}{T}t\right)x, \dot{\epsilon}_0 \sin\left(\frac{2\pi}{T}t\right)y, 0\right] \tag{1}$$

where $\dot{\epsilon}_x(t)$ and $\dot{\epsilon}_y(t)$ are the time-dependent fluid strain rates in the x and y directions, x and y are distances measured from the stagnation point, $\dot{\epsilon}_0$ is the maximum strain rate amplitude, and T is the cycle period.

In this work, we fabricate single-layer polydimethylsiloxane (PDMS)–based microfluidic devices using standard soft lithography techniques [35]. Microdevices contain cross-slot channel geometries with a 400-μm channel width and 90-μm channel height [36]. Channel dimensions are much larger compared to the equilibrium coil size ($R_g \approx 0.7$ μm [37]) and contour length ($L = 21.5$ μm [38]) for fluorescently labeled λ-DNA, such that confinement effects can safely be ignored. Following device fabrication, we use particle tracking velocimetry (PTV) to determine the fluid strain rates as a function of the input pressure. This process is repeated by using both the top-bottom channels and left-right channels as inlets in separate experiments [Fig. 1(b)], which ensures symmetry in flow calibration. Particle tracking was also used to determine the characteristic response time δt

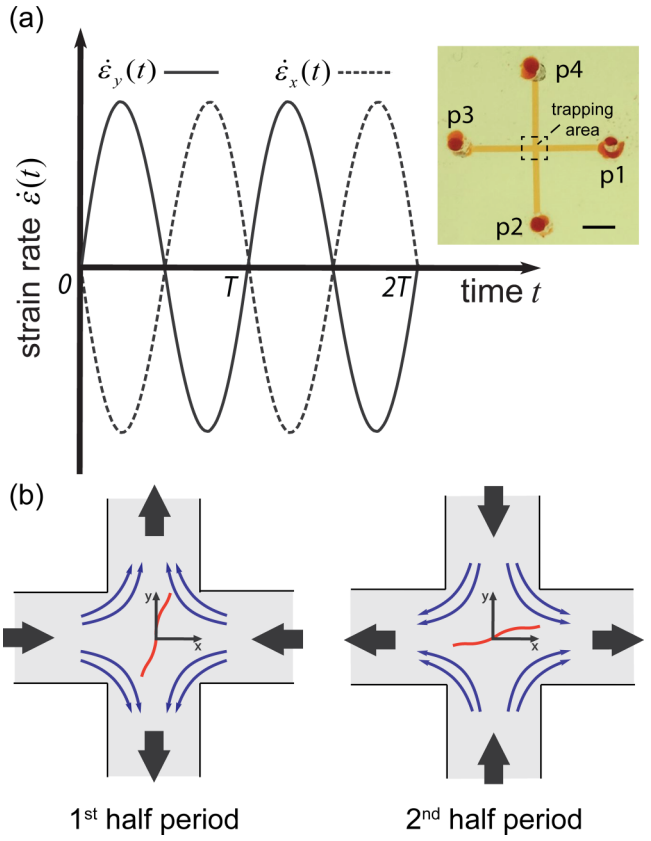

FIG. 1. Single polymer dynamics in large-amplitude oscillatory extension (LAOE). (a) Sinusoidal strain rate input for single polymer LAOE in orthogonal directions. Inset: optical micrograph of PDMS-based microfluidic cross-slot device showing four inlet ports ($p1$-$p4$). Scale bar: 2 mm. (b) Schematics of time-dependent sinusoidal oscillatory extensional flow inside the cross-slot device.

for actuating fluid flow in response to a sudden and large pressure change in the microdevice. The finite response time arises due to the elasticity of PDMS and flow lines [39]. For the extreme case of a large step pressure impulse of 1.2 psi (corresponding to a strain rate increase from $\dot{\epsilon} = 0$ to $\sim 1\ \mathrm{s}^{-1}$), we determined that $\delta t \approx 1$ s. However, during the course of LAOE experiments, the pressure is continuously varying with small incremental changes, for which we generally encounter much smaller characteristic response times. Nevertheless, we choose cycle time T to be much larger than the maximum characteristic rise time δt for fluid response in microdevices corresponding to a large step input flow rate.

Using this approach, we studied the dynamics of single λ-phage DNA molecules in LAOE. λ-DNA (48.5 kbp, 21.5-μm stained contour length [38], New England Biolabs) was fluorescently labeled with YOYO-1 dye (Molecular Probes, Thermo Fisher) at a dye-base pair ratio of 1:4 as previously reported [24]. The imaging buffer contained 30 mM Tris/Tris-HCl (pH 8.0), 2 mM ethylenediaminetetraacetic acid (EDTA), and 5 mM NaCl. Additionally, photobleaching was minimized by adding a mixture of glucose (5 mg/mL), glucose oxidase (0.05 mg/mL), catalase (0.01 mg/mL), and 4% (v/v) β-mercaptoethanol into the imaging buffer solution. Finally, sucrose (60% w/w) was added to adjust the solvent viscosity of the imaging buffer to 48.5 ± 1 cP at room temperature (22.5 °C). The DNA concentration c_{DNA} in the imaging buffer was ultradilute, such that $c_{\mathrm{DNA}} \approx 10^{-5} c^*$, where c^* is the overlap concentration of λ-DNA. An inverted microscope

(IX71, Olympus) equipped for epifluorescence and an electron multiplying charge coupled device (EMCCD) camera (iXon, Andor Technology) were used to acquire single molecule fluorescence images. A 100-W mercury arc lamp (USH102D, UShio) was used as the excitation light source, in conjunction with a neutral density filter (Olympus), a 482 ± 18 nm band-pass excitation filter (FF01-482/18-25, Semrock), and a 488-nm single-edge dichroic mirror (Di01-R488-25 × 36, Semrock) in the illumination path. Emitted light is collected by a 1.45-NA, 100× oil immersion objective (UPlanSApo, Olympus) following a 488-nm-long pass barrier filter (BLP01-488R-25, Semrock). The longest polymer relaxation time τ is determined by observing single polymers relax from high extension following cessation of flow. In this way, the average squared polymer extension $\langle l(t)l(t)\rangle$ is fit to a single exponential decay for $l/L < 0.3$, such that $\langle l(t)l(t)\rangle = A\exp(-t/\tau) + B$, where τ is the longest relaxation time and A and B are fitting constants. In this work, we found $\tau = 4.5 \pm 0.1$ s in 48.5 ± 1 cP imaging buffer, which agrees well with prior studies on single DNA molecule relaxation in viscous buffers [40].

III. BROWNIAN DYNAMICS SIMULATION

We used a coarse-grained bead-spring model to simulate the dynamics of single polymer chains in LAOE. A detailed description of the model and simulation procedure has been previously published [24,30,41]. In brief, a polymer chain is modeled by a series of beads or points of hydrodynamic drag connected by entropic springs. The equation of motion for each bead i in the N-particle system is described by the Langevin equation. Here, we focus on time scales much longer than the particle momentum relaxation time. Under this assumption, particle momenta relax much faster than particle configurations such that

$$m_i\dot{\mathbf{v}}_\mathbf{i} = \mathbf{F}_i^B + \mathbf{F}_i^d + \mathbf{F}_i^s + \mathbf{F}_i^{EV} \simeq 0, \tag{2}$$

where subscript i denotes bead i, m_i is the mass of bead i, $\mathbf{F}_i^B$ is the Brownian force exerted on bead i, $\mathbf{F}_i^d$ is the hydrodynamic drag force on bead i due to its movement in a viscous solvent, $\mathbf{F}_i^s$ is the entropic spring force, and $\mathbf{F}_i^{EV}$ is the force due to intramolecular excluded volume (EV) interactions. Equation (2) can be recast into a set of stochastic differential equations (SDEs) for the positions of beads $i = 1$ to N:

$$d\mathbf{r}_i = \left(\boldsymbol{\kappa}\cdot\mathbf{r}_i + \sum_{j=1}^{N}\frac{\partial \mathbf{D}_{ij}}{\partial \mathbf{r}_j} + \sum_{j=1}^{N}\frac{\mathbf{D}_{ij}\cdot\mathbf{F}_j}{kT}\right)dt + \sqrt{2}\sum_{j=1}^{i}\alpha_{ij}d\mathbf{W}_i \tag{3}$$

where $d\mathbf{W}_i$ represents an independent three-dimensional Wiener process [42] whose value is given by the product of $\sqrt{dt}$ and a randomly distributed Gaussian vector $\mathbf{n}_i$ with zero mean and unit variance, $\boldsymbol{\kappa}$ denotes the time-dependent velocity gradient tensor for oscillatory planar extensional flow:

$$\boldsymbol{\kappa} = \begin{pmatrix} -\dot{\epsilon}_0 \sin\left(\frac{2\pi}{\tilde{T}}t\right) & 0 & 0 \\ 0 & \dot{\epsilon}_0 \sin\left(\frac{2\pi}{\tilde{T}}t\right) & 0 \\ 0 & 0 & 0 \end{pmatrix}, \tag{4}$$

where $\tilde{T}$ is the dimensionless period. In Eq. (3), $\mathbf{D}_{ij}$ is chosen to be the Rotne-Prager-Yamakawa (RPY) tensor which is positive semidefinite for all polymer configurations [43]. The RPY tensor $\mathbf{D}_{ij}$ is related to the coefficient tensor $\boldsymbol{\alpha}_{ij}$ by

$$\mathbf{D}_{ij} = \sum_{l=1}^{N}\boldsymbol{\alpha}_{il}\cdot\boldsymbol{\alpha}_{jl}. \tag{5}$$

Equation (3) is nondimensionalized using characteristic time t_s, length l_s, and force scales F_s. Briefly, time is nondimensionalized by the longest relaxation time of a Hookean dumbbell $t_s = \zeta/4H_s$, where ζ is the hydrodynamic drag coefficient on a bead and H_s is the entropic spring constant for a Hookean spring given by $H_s = 3kT/N_{k,s}b_k^2$ [44]. The Kuhn step size is denoted as b_k, the number of Kuhn steps per entropic spring is $N_{k,s}$, and thermal energy is kT. The characteristic

length scale $l_s = \sqrt{kT/H_s}$ is chosen to be the average equilibrium length of a Hookean dumbbell, and the characteristic force is $F_s = \sqrt{kTH_s}$. Each entropic spring represents a subportion of the entire polymer chain, such the total number of Kuhn steps in the polymer is $N_{k,\mathrm{tot}} = (N-1)N_{k,s}$. The internal configuration of bead-spring polymer chain is described by a series of connector vectors $\mathbf{Q}_i = \mathbf{r}_{i+1} - \mathbf{r}_i$ wherein i ranges from 1 to $N-1$. Using this formulation, Eq. (3) can be recast into dimensionless form and written in terms of the spring connector vector:

$$d\mathbf{Q}_i = \left[\mathrm{Pe}(\boldsymbol{\kappa}\cdot\mathbf{Q}_i) + \sum_{j=1}^{N}(\mathbf{D}_{i+1,j} - \mathbf{D}_{i,j})\left(\mathbf{F}_j^E + \mathbf{F}_j^{EV}\right)\right]dt + \sqrt{2}\sum_{j=1}^{i+1}(\boldsymbol{\alpha}_{i+1,j} - \boldsymbol{\alpha}_{i,j})\cdot d\mathbf{W}_j, \quad (6)$$

where $1 \leqslant i \leqslant N-1$ and $\mathbf{F}_j^E$ is the total entropic spring force exerted on bead j given by

$$\mathbf{F}_j^E = \begin{cases} \mathbf{F}_1^s & \text{if } j = 1 \\ \mathbf{F}_j^s - \mathbf{F}_{j-1}^s & \text{if } 1 < j < N \\ -\mathbf{F}_{N-1}^s & \text{if } j = N \end{cases}. \quad (7)$$

The Marko-Siggia or wormlike chain (WLC) spring force [45] is employed for $\mathbf{F}_i^s$ to model the entropic force between two adjacent beads and is appropriate for double-stranded DNA:

$$\mathbf{F}_i^s = \frac{kT}{b_k}\left\{\frac{1}{2}\frac{1}{[1-(Q/Q_0)]^2} - \frac{1}{2} + \frac{2Q}{Q_0}\right\}\frac{\mathbf{Q}_i}{Q_0}, \quad (8)$$

where Q is the scalar magnitude of the connector vector $\mathbf{Q}_i$ and Q_0 is the maximum extensibility of a spring given by $Q_0 = N_{k,s}b_k$. The bead P é clet number is defined as $\mathrm{Pe} = \dot{\epsilon}_0\zeta/4H_s$, and the dimensionless velocity gradient tensor can be expressed as $\boldsymbol{\kappa} = \sin(2\pi t/\tilde{T})(-\boldsymbol{\delta}_{m1}\boldsymbol{\delta}_{n1} + \boldsymbol{\delta}_{m2}\boldsymbol{\delta}_{n2})$, where $\boldsymbol{\delta}_{mn}$ is the second order isotropic tensor. The maximum Weissenberg number Wi_0 is given by $\mathrm{Wi}_0 = \mathrm{Pe}\tilde{\tau}$ and the Deborah number is $\mathrm{De} = \tilde{\tau}/\tilde{T}$, where $\tilde{\tau}$ is the dimensionless longest relaxation time for the bead-spring chain.

For bead-spring chains with intramolecular hydrodynamic interactions (HI) and excluded volume (EV) interactions, a hydrodynamic interaction parameter h^* is defined as [42]

$$h^* = a\sqrt{\frac{H_s}{\pi kT}}, \quad (9)$$

where a is the hydrodynamic bead radius in the RPY tensor. Excluded volume interactions are modeled using a well-behaved generalized function with a narrow Gaussian potential [41], which is convenient for implementing in BD simulations:

$$U_{ij}^{EV} = \frac{1}{2}\nu kT N_{k,s}^2\left(\frac{3}{4\pi R_{g,\mathrm{sub}}^2}\right)^{3/2}\exp\left[-\frac{3r_{ij}^2}{4R_{g,\mathrm{sub}}^2}\right], \quad (10)$$

where U_{ij}^{EV} is the EV potential between beads i and j, ν is the EV parameter, $R_{g,\mathrm{sub}} = \sqrt{(N_{k,s}b_k)^2/6}$ is the radius of gyration of a subsection of the chain, r_{ij} is the scalar magnitude of $\mathbf{r}_{ij}$, and $\mathbf{r}_{ij}$ is the vector between beads i and j defined by $\mathbf{r}_{ij} = \mathbf{r}_j - \mathbf{r}_i$. Using this expression, the dimensionless EV force $\mathbf{F}_i^{EV}$ on bead i in Eq. (6) is given by [30]

$$\mathbf{F}_i^{EV} = -\sum_{j=1;i\neq j}^{N}\frac{9\sqrt{3}z}{2}\exp\left[-\frac{3r_{ij}^2}{2}\right]\mathbf{r}_{ij}, \quad (11)$$

where quantity z is defined in terms of the EV parameter ν given by [42,46]

$$z = \left(\frac{1}{2\pi}\right)^{3/2}\tilde{\nu}N_{k,s}^2, \quad (12)$$

where $\tilde{\nu} = \nu/l_s^3$ is the dimensionless EV parameter [42,46].

For free-draining bead-spring chains without EV interactions, the hydrodynamic drag on all beads is constant and the excluded volume force $\mathbf{F}_i^{EV} = 0$. In the case of free-draining chains with no EV, Eq. (6) reduces to

$$d\mathbf{Q}_i = \left[\mathrm{Pe}(\boldsymbol{\kappa}\cdot\mathbf{Q}_i) + \tfrac{1}{4}\left(\mathbf{F}_{i+1}^{E} - \mathbf{F}_i^{E}\right)\right]dt + \tfrac{1}{2}(d\mathbf{W}_{i+1} - d\mathbf{W}_i). \tag{13}$$

The SDEs described in Eqs. (6) and (13) were solved using an efficient second-order predictor-corrector algorithm [30,44,47]. In this way, the equation of motion is solved to determine the set of connector vectors $\mathbf{Q}_i$ as a function of time. Before initiating flow, all polymer chains in the simulated ensemble were first allowed to equilibrate for 10 $\tilde{\tau}$ to ensure random initial chain conformations. Finally, model parameters were systematically chosen to match the experimental polymer contour length L and relaxation time τ for λ-DNA molecule in the 48.5 ± 1 cP imaging buffer. For simulations with HI and EV, we used the following parameters: number of springs $N_s = 9$, number of Kuhn steps per spring $N_{k,s} = 22$, Kuhn length $b_k = 0.106\,\mu$m, bead radius $a = 0.344\,\mu$m, EV parameter $\nu = 0.0508\,\mu\mathrm{m}^3$, and HI parameter $h^* = 0.196$. These parameter values are chosen to be in accordance with previously published multimode bead-spring simulations with HI and EV that accurately capture the equilibrium and nonequilibrium dynamic behavior of λ-DNA in flow [41], including steady-state fractional extension in shear and extensional flow. We also verified that these parameter choices faithfully reproduce the experimental longest relaxation time τ. The BD simulation gives the dimensionalized longest polymer relaxation time $\tau = 4.3 \pm 0.1$ s compared to $\tau = 4.5 \pm 0.1$ s from experiments. For the free-draining (FD) bead-spring model, we chose $N_s = 15$ and $N_{k,s} = 10$. We note that $N_s = 15$ for free-draining chains is slightly different than the value used for HI/EV chains; however, we generally found that small differences in coarse-graining levels for FD chains do not yield significant differences in dynamics at this level of discretization. For FD simulations, the drag coefficient ζ on each bead is chosen so that the longest polymer relaxation time from simulations matches experimental data.

IV. RESULTS AND DISCUSSION

Using a combination of single molecule experiments and BD simulations, we directly observe the dynamics of single polymers in steady-state LAOE as a function of the flow strength and cycle frequency. The Weissenberg number $\mathrm{Wi}_0 = \dot{\epsilon}_0\tau$ is the maximum dimensionless flow strength during one input cycle, defined as the ratio of the longest polymer relaxation time τ to the maximum characteristic fluid time scale $\dot{\epsilon}_0^{-1}$. The Deborah number $\mathrm{De} = \tau/T$ is defined as the ratio of the longest polymer relaxation time τ to the characteristic cycle time scale T. In this work, we only consider steady-state LAOE, which refers to single chain dynamics after the initial transient phase of flow dynamics corresponding to the onset of oscillatory flow. In this way, we discard the polymer response during the startup period of LAOE [48], essentially focusing on times $t \gg T$ and $t \gg \tau$. Compared to simple shear flow or linear mixed flows, steady extensional flow is considered to be a strong flow with zero rotational character, which is highly efficient in unravelling and aligning polymer molecules [15]. From this view, LAOE is transient flow type that is intrinsically strong and capable of high degrees of polymer stretching, yet will generally yield no long-time stable steady state in polymer extension. Hence, it is important to note that steady-state LAOE is defined in terms of characteristic time scales, rather than the conventional definition of steady-state polymer chain extension or saturation in flow birefringence over long times in steady extensional flows [49].

Single molecule experimental LAOE trajectories are shown in Fig. 2(a), where polymer fractional extension l/L is plotted over 5 units of polymer longest relaxation time τ at $\mathrm{Wi}_0 = 6.5$ and $\mathrm{De} = 0.45$. Here, we define fractional extension l/L as the maximum projected extension l of a single polymer along any direction in the x-y plane relative to the polymer contour length L. At $\mathrm{Wi}_0 = 6.5$, the maximum flow strength far exceeds the critical Wi at the coil-stretch transition in steady extensional flows [27,50], thereby resulting in high degrees of deformation and a strong nonlinear response. Interestingly, the maximum projected extension $l/L \approx 0.6$, which is less than the value expected for steady extensional flows ($\mathrm{De} = 0$) at $\mathrm{Wi} = 6.5$ [27]. This observation suggests that

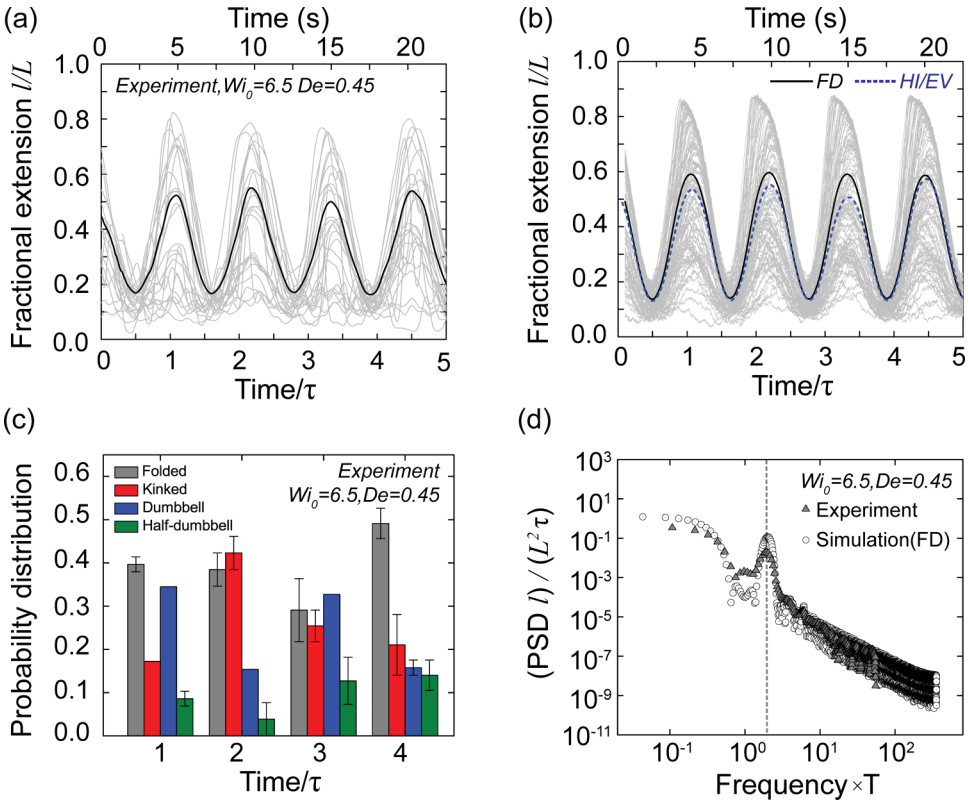

FIG. 2. Single polymer dynamics in LAOE from experiments and simulations. (a) Experimental trajectories of maximum projected polymer fractional extension l/L over the x-y plane for an ensemble of >30 individual molecules (black) overplotted with single polymer trajectories (gray) at $\mathrm{Wi}_0 = 6.5$ and $\mathrm{De} = 0.45$. (b) Maximum projected polymer fractional extension l/L from free-draining BD simulations at $\mathrm{Wi}_0 = 6.5$ and $\mathrm{De} = 0.45$ for an ensemble average over 250 molecules (black) overplotted with single polymer trajectories (gray). Also shown is the ensemble average fractional extension l/L from BD simulations with HI and EV (dashed blue line). (c) Probability distribution of four experimentally observed molecular configurations (folded, kinked, dumbbell, and half-dumbbell) in LAOE at $\mathrm{Wi}_0 = 6.5$ and $\mathrm{De} = 0.45$. (d) Power spectral density of polymer extension l from experiments and simulations at $\mathrm{Wi}_0 = 6.5$ and $\mathrm{De} = 0.45$.

the probing frequency De plays a significant role on polymer dynamics in LAOE, even for $\mathrm{De} < 1$, wherein the polymer chain might be expected to have sufficient time to respond to flow deformation because the cycle time T is longer than the polymer relaxation time τ for these conditions ($T > \tau$ for $\mathrm{De} < 1$).

Experimental results show good agreement with predictions from free-draining (FD) multimode BD simulations and BD simulations with HI/EV interactions [Fig. 2(b)]. The FD simulation results slightly overpredict the maximum polymer extension at the peaks and slightly underpredict at the valleys, while simulations with HI and EV interactions capture the dynamics nearly quantitatively.

LAOE experiments reveal marked heterogeneity in polymer fractional extension upon stretching in both the x and y directions, which is also captured by the simulations. We identified four distinct molecular conformations for polymer stretching in LAOE: dumbbells, half-dumbbells, folds, and kinks. In particular, polymer molecules adopting a dumbbell, half-dumbbell, or kinked configuration stretch more rapidly than average and achieve extensions that generally exceed the average fractional extension. On the other hand, polymer molecules with folded conformations are internally constrained and stretch slower than average and generally achieve lower degrees of

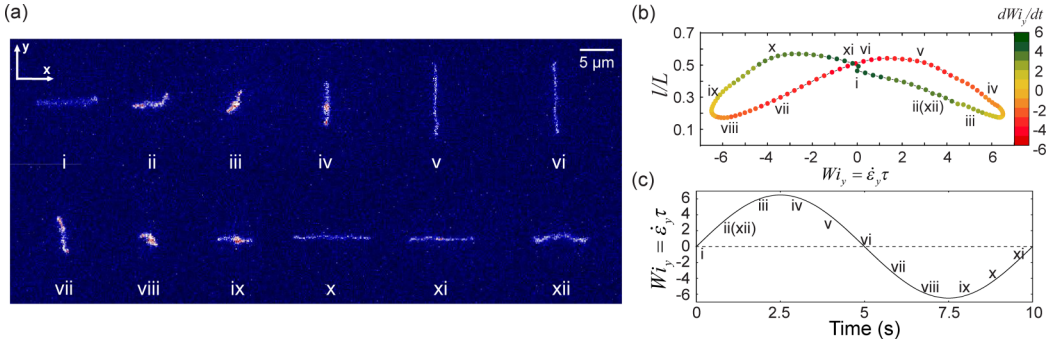

FIG. 3. Single polymer LAOE at $\mathrm{Wi}_0 = 6.5$ and $\mathrm{De} = 0.45$. (a) A series of single polymer snapshots is used to characterize polymer motion during one sinusoidal strain rate input cycle. The time between each snapshot is 1 s. (b) Experimental single polymer Lissajous plot showing the average projected fractional extension l/L as a function of $\mathrm{Wi}_y(t)$ at $\mathrm{Wi}_0 = 6.5$ and $\mathrm{De} = 0.45$. The color scale denotes the rate of change of the strain rate input function $d\mathrm{Wi}_y/dt$. (c) Experimental strain rate input function with period $T = 10$ s.

fractional extension. The probability of occurrence of distinct polymer conformations is shown in Fig. 2(c) for a series of half cycles at $\mathrm{Wi}_0 = 6.5$ and $\mathrm{De} = 0.45$. These results show that approximately half of the molecules are in configurations exhibiting fast stretching dynamics (kinked, dumbbell, half-dumbbell) while the other half are folded conformations with slow dynamics. Of course, these results will quantitatively depend on Wi_0 and De, but generally speaking, these conformations are fairly consistent across the regime of high flow rates $\mathrm{Wi}_0 > 1$ and long cycle times $\mathrm{De} < 1$, such that the flow will induce high degrees of polymer stretch and the cycle times are long enough for the polymer to respond during one cycle. Interestingly, the molecular conformations observed in LAOE are similar to those observed in steady extensional flow [27,28]; however, their relative proportions and dynamic transitions between conformations in transient LAOE are quite different compared to steady extension and are unique to this flow type.

The characteristic periodic cycle of polymer motion was further characterized by the power spectral density (PSD) of projected chain extension $l(t)$. The PSD is defined as

$$P(f) = \int_{-\infty}^{\infty} C(\lambda)_{l,l} e^{-2i\pi f\lambda} d\lambda \tag{14}$$

where f is the frequency, $i = \sqrt{-1}$, and $C(\lambda)_{l,l}$ is the autocorrelation function of $l(t)$ defined as

$$C(\lambda)_{l,l} = \langle l(t) l(t+\lambda) \rangle, \tag{15}$$

where t denotes time, λ is the offset time, and $\langle \cdot \rangle$ corresponds a time-averaged quantity [51]. The PSD is nondimensionalized by $L^2\tau$, where L is the polymer contour length and τ is the longest relaxation time. As shown in Fig. 2(d), we find good agreement between the PSD of fractional extension from experiments and simulations. Distinct peaks are observed for both PSDs at a dimensionless frequency of $fT = 2$, which indicates that the autocorrelation of the polymer fractional extension exhibits a peak at half the sinusoidal strain rate cycle period. In other words, under these flow conditions ($\mathrm{Wi}_0 = 6.5$ and $\mathrm{De} = 0.45$), polymer chains reach the maximum stretch twice during one strain rate input cycle.

To further understand transient polymer dynamics in LAOE, we examined a series of single polymer snapshots over the course of one strain rate input cycle at $\mathrm{Wi}_0 = 6.5$ and $\mathrm{De} = 0.45$ [Fig. 3(a)]. These images show that the maximum extension occurs along both the y axis and x axis during one cycle period, because these axes switch roles as the extensional and compressional axes exactly once per one LAOE period. To further quantify LAOE dynamics, we construct single polymer Lissajous curves in LAOE [Fig. 3(b)], which are defined as a plot of the average periodic fractional extension l/L at steady state as a function of the transient $\mathrm{Wi}_y(t)$ in the y direction, such

that $\mathrm{Wi}_y(t) = \dot{\epsilon}_y(t)\tau$. For reference, the strain rate input $\mathrm{Wi}_y(t)$ is also plotted in Fig. 3(c) as a function of time t, where the experimental strain rate input period $T = 10$ s. For reference, the labels on the single molecule snapshots (i–xi) in Fig. 3(a) correspond to the labels in Figs. 3(b) and 3(c).

It is instructive to examine polymer chain dynamics over one full cycle in LAOE (Fig. 3). The cycle begins when a polymer chain starts from a stretched state i along the x axis with $l/L \approx 0.45$ at $t = 0$ s. Next, $\mathrm{Wi}_y(t)$ begins to increase, and the polymer chain is compressed along the x axis while rotating towards the y axis, which is the new extensional axis, as shown in state ii. As $\mathrm{Wi}_y(t)$ continues to increase in magnitude, the polymer chain is quickly compressed into a compact conformation (state iii) before being aligned along the extensional axis (state iv). After the quarter cycle at $t = 2.5$ s, the strain rate $\mathrm{Wi}_y(t)$ begins to decrease; however, the polymer chain continues to be stretched along the y axis into state v. After $t = 4$ s, the chain length saturates (or slightly decreases) due to the reduction in $\mathrm{Wi}_y(t)$. After $t = 5$ s, the polymer follows a similar dynamic pathway entering the second half period of the strain rate input, and the cycle repeats in the opposite direction as the roles of the extensional and compressional axes are switched. Of course, the full cycle repeats when a new strain rate input period starts, and state xii at the end of one cycle corresponds to the first compressed polymer conformation during the next deformation cycle (state ii).

We further investigated how the shapes of the Lissajous curves vary as a function of the flow strength Wi_0 and the cycle frequency De using experiments and BD simulations [Figs. 4(a)–4(c)]. Here, we maintained the flow strength at $\mathrm{Wi}_0 \approx 5$ and changed the probing frequency from $\mathrm{De} = 0.1$ to $\mathrm{De} = 0.45$. We found that single polymer Lissajous curves open up from an arch shape at $\mathrm{De} = 0.45$ and $\mathrm{Wi}_0 = 6.5$ [Fig. 4(c)], to a bow-tie shape at $\mathrm{De} = 0.25$ and $\mathrm{Wi}_0 = 5$ [Fig. 4(b)], and finally to a butterfly shape at $\mathrm{De} = 0.1$ and $\mathrm{Wi}_0 = 5$ [Fig. 4(a)]. We distinguish the bow-tie shape from the butterfly shape by examining the line tangent to the Lissajous curve, noting that the butterfly shape exhibits a sharp corner or cusp at the extreme values of Wi. In general, we observe good agreement between BD simulations and experiments across a wide range of flow strengths Wi_0 and cycle frequencies De. Interestingly, the free-draining simulations appear to capture the experimental dynamics more quantitatively at lower frequencies De (corresponding to longer cycle times T). At high frequency [$\mathrm{De} = 0.45$, Fig. 4(c)], the principal axes of extension-compression switch more rapidly relative the polymer relaxation time, which results in polymer chains residing in more compact intermediate states across the cycle period. These dynamics appear to be better captured by BD simulations with HI/EV, which is consistent with the dominant role of intramolecular hydrodynamic interactions and excluded volume interactions for a more compact polymer chain. On the other hand, at relatively low probing frequency [$\mathrm{De} = 0.1$, Fig. 4(a)], the polymer has more time to respond to fluid deformation in a cycle period and remains in highly extended states for longer periods of time during each cycle, which appears to be well modeled by free-draining BD simulations. It is worth mentioning that the HI and EV parameters for the HI/EV BD simulation are fit to match near-equilibrium parameters (longest relaxation time and center-of-mass diffusivity) [30,41], which may partially explain the better agreement of the HI/EV model at high frequency De. Nevertheless, from a broad perspective, both models (FD and HI/EV) sufficiently capture the dynamics in LAOE and any differences are fairly minor.

We further determined the polymer contribution to the total stress $\boldsymbol{\tau}^p$ from BD simulations using the Kramers expression [3]. For bead-spring polymer models with intramolecular HI and EV interactions, the polymer contribution to the total stress tensor $\boldsymbol{\tau}^p$ is defined as [3]

$$\frac{\boldsymbol{\tau}^p}{nkT} = \sum_{k=1}^{N_s} \left\langle \mathbf{Q}_k \mathbf{F}_k^s \right\rangle - \sum_{j=1}^{N} \sum_{k=1}^{N_s} B_{jk} \left\langle \mathbf{Q}_k \mathbf{F}_j^{EV} \right\rangle - N_s \boldsymbol{\delta}, \tag{16}$$

where the quantity nkT is used to render $\boldsymbol{\tau}^p$ dimensionless. Here, n denotes the number density of the polymer chains in the ensemble and B_{jk} is a matrix defined as

$$B_{jk} = \begin{cases} \frac{k}{N} & \text{if } k < j \\ -\left(1 - \frac{k}{N}\right) & \text{if } k \geqslant j \end{cases}. \tag{17}$$

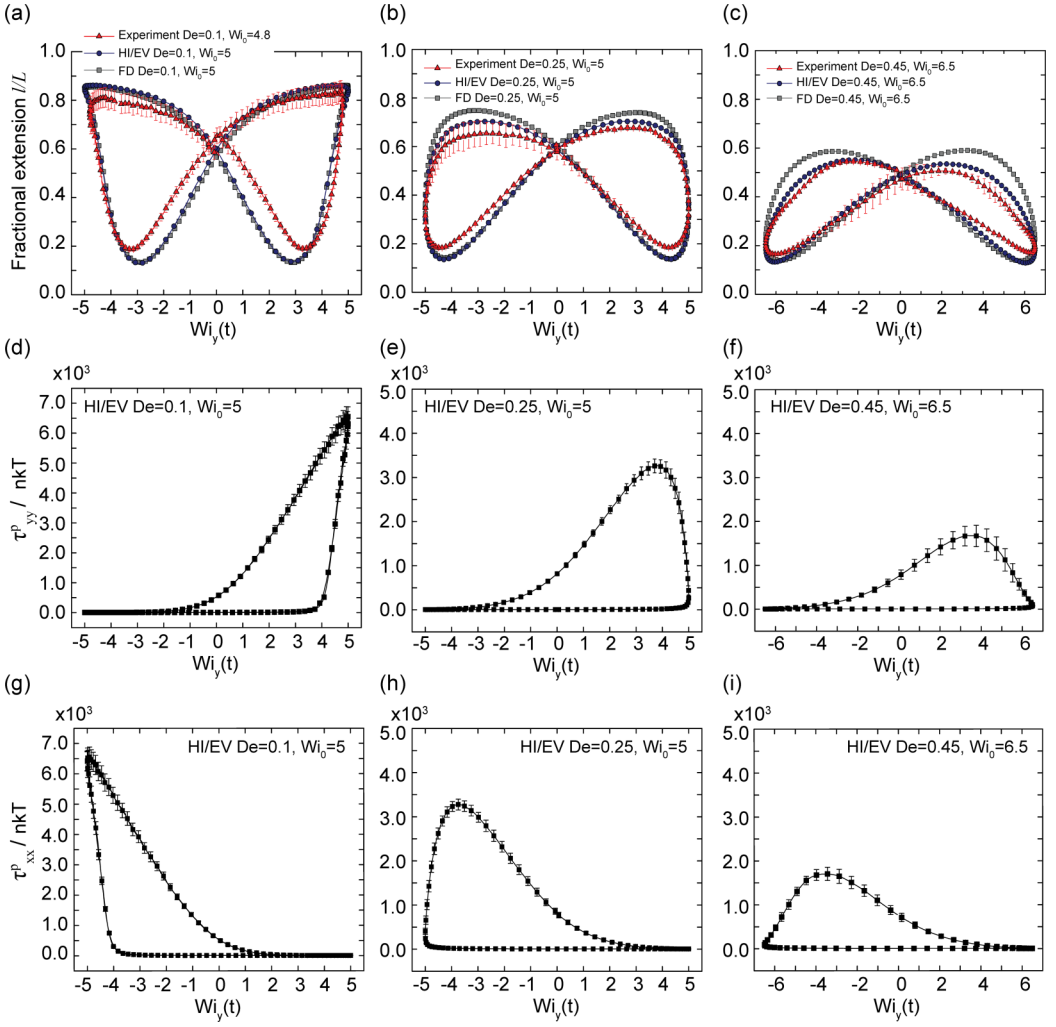

FIG. 4. Single polymer Lissajous curves from experiments, BD simulations with hydrodynamic interactions (HI) and excluded volume (EV) interactions, and free-draining (FD) BD simulations at (a) $\mathrm{De} = 0.1$ and $\mathrm{Wi}_0 = 5$, (b) $\mathrm{De} = 0.25$ and $\mathrm{Wi}_0 = 5$, and (c) $\mathrm{De} = 0.45$ and $\mathrm{Wi}_0 = 6.5$. Polymer contribution to the total stress along the yy direction calculated from Kramers expression at (d) $\mathrm{De} = 0.1$ and $\mathrm{Wi}_0 = 5$, (e) $\mathrm{De} = 0.25$ and $\mathrm{Wi}_0 = 5$, and (f) $\mathrm{De} = 0.45$ and $\mathrm{Wi}_0 = 6.5$. Polymer contribution to the total stress along the xx direction calculated from Kramers expression at (g) $\mathrm{De} = 0.1$ and $\mathrm{Wi}_0 = 5$, (h) $\mathrm{De} = 0.25$ and $\mathrm{Wi}_0 = 5$, and (i) $\mathrm{De} = 0.45$ and $\mathrm{Wi}_0 = 6.5$.

The polymer contribution to the total stress along the y direction τ^p_{yy} is shown in Figs. 4(d)–4(f), and the polymer contribution to the stress in the x direction τ^p_{xx} is shown in Figs. 4(g)–4(i). During the first half of the LAOE cycle with $\mathrm{Wi}_y(t) > 0$, the change of τ^p_{yy} with respect to flow strength is in accordance with the change in polymer projected extension such that the polymer is highly stretched along the y direction ($\tau^p_{yy} \gg 0$) and not appreciably stretched along the x direction ($\tau^p_{xx} \approx 0$). Entering the second half of the LAOE cycle with $\mathrm{Wi}_y(t) < 0$, the polymer begins to stretch along the x direction, such that τ^p_{yy} gradually decreases to zero and τ^p_{xx} increases to large values, which essentially follows the opposite path compared to the first half-cycle. The peak values in the polymer contribution to the total stress τ^p_{yy} and τ^p_{xx} show that the polymer contributes most to the total stress at the maximum chain extension during each LAOE half-cycle.

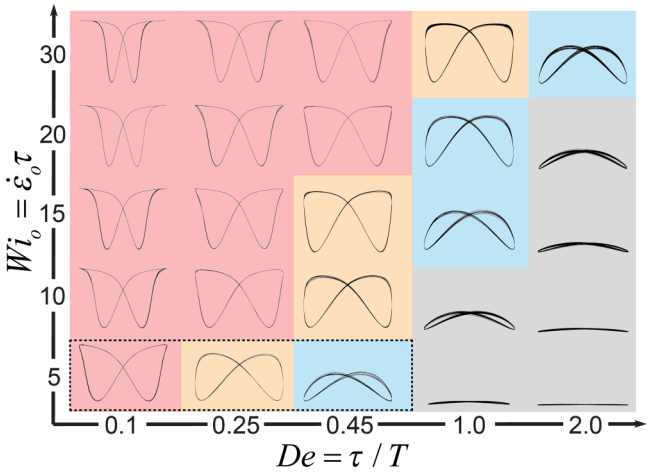

FIG. 5. Single polymer Lissajous curves showing subplots of average transient fractional extension l/L as a function of the transient flow strength $\mathrm{Wi}_y(t)$. Individual Lissajous curves are plotted over the two-dimensional Pipkin space as functions of the maximum flow strength Wi_0 and probing frequency De. Results are shown from free-draining BD simulations. The gray region represents line shapes, the blue region represents arch shapes, the orange region represents bow-tie shapes, and the red region represents butterfly shapes.

We further explored LAOE dynamics over a broad range of Wi and De known as Pipkin space (Fig. 5). In bulk rheology, Pipkin space generally refers to the two-dimensional space recovered by plotting the transient stress-strain (or stress-strain rate) response of a material as a series of curves as functions of flow rate Wi and probing frequency De [52]. Here, we construct a series of single molecule Lissajous curves for LAOE in Pipkin space (Fig. 5), wherein subplots show average fractional chain extension l/L versus flow rate $\mathrm{Wi}_y(t)$ across a broad range of parameters Wi_0 and De. For simplicity, we only consider free-draining BD simulations for exploring Pipkin space, given that HI/EV was shown to have a fairly minor effect on dynamics across a limited range of Wi and De [Figs. 4(a)–4(c)]. Moreover, we emphasize the single molecule nature of these experiments and simulations by plotting Lissajous curves as fractional extension l/L rather than polymer stress; however, one could construct equivalent curves based on polymer contribution to stress (τ_{yy}^p or τ_{xx}^p) if so desired.

As shown in Fig. 5, the horizontal axis De denotes the probing frequency ranging from $\mathrm{De} = 0.1$ to $\mathrm{De} = 2$. At low frequencies $\mathrm{De} < 1$, the characteristic cycle time is longer than the polymer relaxation time, whereas at high frequencies $\mathrm{De} > 1$, the characteristic cycle time is shorter than the polymer relaxation time. Interestingly, we found that the Lissajous curves in this parameter regime can be categorized into four general shapes: line, arch, bow-tie, and butterfly. We note that the butterfly, bow-tie, and arch shapes were observed in single polymer experiments [Figs. 4(a)–4(c), respectively]. Using this scheme, a line is observed at high De across a wide range of Wi_0 (e.g., at $\mathrm{De} = 2$ for $\mathrm{Wi}_0 \leqslant 20$ and at $\mathrm{De} = 1$ for $\mathrm{Wi}_0 \leqslant 10$). A line shape opens up to an arch upon increasing the flow strength or decreasing the probing frequency (e.g., at $\mathrm{De} = 1$ for $\mathrm{Wi}_0 = 10$–20). For the arch classification, the maximum projected extension generally does not exceed $l/L \approx 0.6$. Upon further decreasing the probing frequency De, an arch opens up to a bow-tie (e.g., at $\mathrm{De} = 0.45$ for $\mathrm{Wi}_0 = 10$–15). For the bow-tie classification, the maximum projected extension is larger compared to the arch shape, but it generally does not exceed $l/L \approx 0.8$ during a cycle. Finally, a bow-tie transforms to a butterfly at lower frequencies or higher flow strengths (e.g., at $\mathrm{De} = 0.25$ for $\mathrm{Wi}_0 > 10$). For the butterfly conformation, polymers are highly stretched in each cycle such that $l/L > 0.8$. Finally, at ultralow frequencies $\mathrm{De} \leqslant 0.1$, all Lissajous curves are butterflies within the range of Wi_0 shown in Fig. 5.

Our results clearly show that LAOE gives rise to complex dynamics, and these results are highly dependent upon the flow strength and cycle period. We further sought to understand whether chain dynamics can be understood by considering the rate of change of strain rate $d\mathrm{Wi}_y/dt$ and the accumulated fluid strain during a cycle $\epsilon(t)$. In this way, we define three stages for each half-cycle ($0 < t < T/2$): an early stage (or compression stage), an intermediate stage (or extension stage), and a late stage (or retraction stage). As an illustrative example, we analyzed chain dynamics over the half cycle $0 < t < T/2$ for the case of $\mathrm{Wi}_0 = 6.5$ and $\mathrm{De} = 0.45$ (Fig. 3). At the onset of a half cycle [time $t = 0$ in Fig. 3(c)], polymer chains are stretched in the x direction. During the early stage in the half cycle, chains begin to become compressed in the x direction and eventually rotate towards the y axis, because the y axis becomes the extensional axis such that $\mathrm{Wi}_y > 0$ for $0 < t < T/2$. We define the early compression stage in the half cycle as beginning at the cross point in the Lissajous curve [$\mathrm{Wi}_y(t) = 0$] and ending at the minimum point in l/L on the Lissajous curve. During the intermediate stage of the half cycle, polymer chains are oriented and stretched along the y axis, which is principal axis of extension. Here, we define the intermediate extension stage of the half cycle from the minimum point to the maximum point in polymer stretch on the Lissajous curve. Finally, during the late stage of the half cycle, polymer chains are still stretched along the y axis, but the strain rate $\mathrm{Wi}_y(t)$ decreases towards zero with a large rate of change $d\mathrm{Wi}_y/dt$, thereby resulting in chain retraction along the y direction. From this view, we define the final retraction stage of the half cycle as beginning at the maximum point in l/L and ending at the cross point on the Lissajous curve.

Using this framework, we quantified transitions between different qualitative shapes in Lissajous plots by decomposing the total accumulated fluid strain during a half cycle $\epsilon_{T/2}$ into three components:

$$\epsilon_{T/2} = \epsilon_1(\mathrm{Wi}_0,\mathrm{De}) + \epsilon_2(\mathrm{Wi}_0,\mathrm{De}) + \epsilon_3(\mathrm{Wi}_0,\mathrm{De}), \tag{18}$$

where ϵ_1, ϵ_2, and ϵ_3 correspond to the fluid strain accumulated during the early (compression), intermediate (extension), and late (retraction) stages of a half cycle. In general, the strain during any of the three stages is determined by

$$\epsilon(\mathrm{Wi}_0,\mathrm{De}) = \int_{t_1}^{t_2} \dot{\epsilon}(t';\mathrm{Wi}_0,\mathrm{De})dt', \tag{19}$$

where the limits of integration t_1 and t_2 are defined by the initial and final points of the early, intermediate, and late stages of the cycle as previously described. Of course, the total accumulated strain during a half cycle $\epsilon_{T/2}$ is constant such that $\epsilon_{T/2} = \mathrm{Wi}_0/\pi\mathrm{De}$, and the total strain during a full cycle is zero ($\epsilon_T = 0$).

Figure 6 plots the accumulated fluid strain during the early [Fig. 6(a)], intermediate [Fig. 6(b)], and late stages [Fig. 6(c)] of a half-cycle as functions of Wi_0 and De. Importantly, the accumulated fluid strains can be used interpret the shapes of the single molecule Lissajous curves shown in Fig. 5. To begin, consider a line shape Lissajous curve observed at $\mathrm{Wi}_0 = 10$ and $\mathrm{De} = 2$. Here, polymer chains experience only small deformations during the cycle. For this case, nearly half of the fluid strain is applied in the early and intermediate stages $\epsilon_1/\epsilon_{T/2} \approx \epsilon_2/\epsilon_{T/2} \approx 0.5$, but essentially zero strain is applied during the late stage such that $\epsilon_3/\epsilon_{T/2} \approx 0$. Upon transitioning from a line to an arch (upon decreasing De), the value of $\epsilon_1/\epsilon_{T/2}$ begins to decrease; however, the retraction strain $\epsilon_3/\epsilon_{T/2} \approx 0$ remains small. For a line or a slightly perturbed arch shape, polymers experience only small deformations and essentially respond as linear elastic objects. We can further consider the transition from an arch to a bow-tie shape, for example, upon decreasing the frequency to $\mathrm{De} = 0.45$ at $\mathrm{Wi}_0 = 10$. Here, the value of $\epsilon_1/\epsilon_{T/2}$ decreases further, whereas $\epsilon_3/\epsilon_{T/2}$ begins to increase as De decreases. From a physical perspective, as De decreases, less fluid strain is required in the early stage to compress polymer chains because polymers are (on average) stretched to larger extensions with an associated larger stored elastic energy. Therefore, as De decreases, the nonlinear elasticity

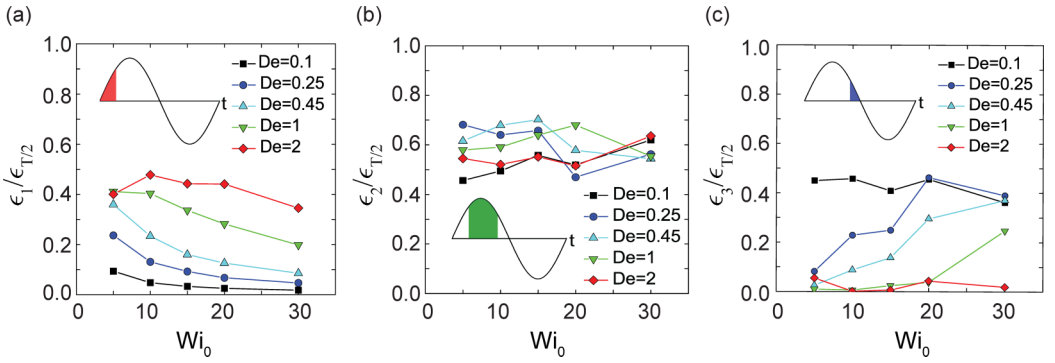

FIG. 6. Quantitative analysis of accumulated fluid strain during the early (compression), intermediate (extension), and late (retraction) stages of a half cycle in LAOE. (a) Fraction of fluid strain accumulated during the early stage of a half sinusoidal cycle $\epsilon_1/\epsilon_{T/2}$. Here, the strain during the early stage ϵ_1 is plotted relative to the total strain during a half cycle $\epsilon_{T/2}$. (b) Fraction of fluid strain accumulated during the intermediate stage of a half sinusoidal cycle $\epsilon_2/\epsilon_{T/2}$. (c) Fraction of fluid strain accumulated during the late stage of a half sinusoidal cycle $\epsilon_3/\epsilon_{T/2}$.

acts in concert with fluid compression during the early stage, thereby resulting in smaller values of $\epsilon_1/\epsilon_{T/2}$.

When a bow-tie transitions to a butterfly shape, for example, upon decreasing the frequency to $\mathrm{De} = 0.1$ at $\mathrm{Wi}_0 = 10$, the amount of compressional strain $\epsilon_1/\epsilon_{T/2}$ in the early stage decreases significantly, whereas the amount of retraction strain $\epsilon_3/\epsilon_{T/2}$ in the late stage significantly increases. In the low-frequency limit, the value of $\epsilon_1/\epsilon_{T/2}$ tends to zero and $\epsilon_3/\epsilon_{T/2}$ approaches $\approx$0.5. From this perspective, the process has essentially completely shifted from the majority of the strain being applied in the early stage (compressional stage) for line shapes to the late stage (retraction stage) for butterfly shapes of the half-cycle period. At the single chain level, an increase in $\epsilon_3/\epsilon_{T/2}$ implies that increasingly larger amounts of strain are required in the late stage to result in chain retraction from the maximum value of l/L to the end of the cycle at $t = T$ ($\mathrm{Wi}_y = 0$). During this phase, polymer chains retract in the opposite direction as the fluid deformation, thereby leading to viscous dissipation into the surrounding solvent.

Using this approach, we qualitatively describe the dynamic behavior of single polymers under LAOE in Pipkin space by classifying different characteristic shapes of Lissajous curves. We further quantitatively characterize the fraction of fluid strain accumulated during the early, intermediate, and late stages of the half cycle of periodic motion in LAOE. Overall, our results are consistent with the notion that polymers behave as linear elastic materials under high probing frequency De (at relatively low flow strength Wi_0), whereas more complex viscoelastic behavior emerges upon decreasing De (at constant Wi_0) or increasing Wi_0 (at constant De).

V. CONCLUSIONS

In this work, we investigate single polymer dynamics in LAOE using a new experimental technique called the Stokes trap, and experimental results are complemented with BD simulations. We show that a single polymer chain experiences continuous cycles of compression, rotation, and extension between the alternating principle axes of compression and extension during periodic oscillatory forcing in extensional flow. Based on BD simulations, our results suggest that intramolecular HI and EV interactions begin to become important at high probing frequencies De. Moreover, we characterize polymer dynamic behavior in LAOE in the context of single polymer Lissajous curves, and we study the effects of dimensionless flow strength Wi_0 and probing frequency De on polymer dynamics by constructing a series of single polymer Lissajous curves over

two-dimensional Pipkin space. We further consider the polymer contribution to the total stress $\boldsymbol{\tau}^p$ in the context of LAOE, which generally shows the same characteristic trends compared to Lissajous plots with respect to flow deformation.

Overall, the approach presented in this work allows for the direct observation of single polymer dynamics in highly controlled and precise time-dependent flows. Moving forward, this approach will serve as a powerful tool in studying the nonequilibrium dynamics of a wide variety of soft deformable particles in controlled time-dependent flows, including vesicles, polymersomes, and coacervates. Thus far, our work has focused on probing the dynamics of single polymers in dilute solutions in the absence of intermolecular interactions or entanglements. Moving forward, we anticipate that this method can be applied to study dynamics in semidilute polymer solutions where both intermolecular polymer interactions and intramolecular HI and EV interactions play a role, and in concentrated polymer solutions where polymer chains are highly entangled. In this way, the rheological behavior obtained from single polymer LAOE can be directly compared to bulk-level experiments on time-dependent flows. Moreover, the Stokes trap and the general single polymer LAOE experiment may prove useful in studying polymers with complex topologies, including comb polymers [53] or ring polymers [54]. From a broad perspective, this technique will open new vistas for studying the dynamics of soft particles, including dynamic shape variations or structural deformations in controlled flows.

ACKNOWLEDGMENTS

We thank Professor Randy H. Ewoldt and Professor Simon A. Rogers for useful discussions and Anish Shenoy for help in implementing the Stokes trap. This work was supported by an National Science Foundation (NSF) CAREER Award (CBET-1254340) to C.M.S.

[1] R. G. Larson, *The Structure and Rheology of Complex Fluids* (Oxford University Press, New York,1999).
[2] G. K. Batchelor, The stress generated in a non-dilute suspension of elongated particles by pure straining motion, J. Fluid Mech. **46**, 813 (1971).
[3] R. B. Bird, R. C. Armstrong, and O. Hassager, *Dynamics of Polymeric Liquids, Volume 2: Kinetic Theory*, 2nd ed. (John Wiley & Sons, York, Canada, 1987).
[4] J. D. Ferry, *Viscoelastic Properties of Polymers*, 3rd ed. (John Wiley & Sons, New York, 1980).
[5] R. B. Bird, R. C. Armstrong, and O. Hassager, *Dynamics of Polymeric Liquids, Volume 1: Fluid Mechanics*, 2nd ed. (John Wiley & Sons, York, Canada, 1987).
[6] A. J. Giacomin and J. M. Dealy, Large-amplitude oscillatory shear, in *Techniques in Rheological Measurement*, edited by A. A. Collyer (Springer, Dordrecht, the Netherlands, 1993), pp. 99–120.
[7] M. Wilhelm, Fourier-transform rheology, Macromol. Mater. Eng. **287**, 83 (2002).
[8] K. Hyun, M. Wilhelm, C. O. Klein, K. S. Cho, J. G. Nam, K. H. Ahn, S. J. Lee, R. H. Ewoldt, and G. H. McKinley, A review of nonlinear oscillatory shear tests: Analysis and application of large amplitude oscillatory shear (LAOS), Prog. Polym. Sci. **36**, 1697 (2011).
[9] M. K. Jung, A. P. R. Eberle, A. K. Gurnon, L. Porcar, and N. J. Wagner, The microstructure and rheology of a model, thixotropic nanoparticle gel under steady shear and large amplitude oscillatory shear (LAOS), J. Rheol. **58**, 1301 (2014).
[10] K. S. Cho, K. Hyun, K. H. Ahn, and S. J. Lee, A geometrical interpretation of large amplitude oscillatory shear response, J. Rheol. **49**, 747 (2005).
[11] R. H. Ewoldt, A. E. Hosoi, and G. H. McKinley, New measures for characterizing nonlinear viscoelasticity in large amplitude oscillatory shear, J. Rheol. **52**, 1427 (2008).
[12] S. A. Rogers and M. P. Lettinga, A sequence of physical processes determined and quantified in large-amplitude oscillatory shear (LAOS): Application to theoretical nonlinear models, J. Rheol. **56**, 1 (2012).

[13] K. Hyun, S. H. Kim, K. H. Ahn, and S. J. Lee, Large amplitude oscillatory shear as a way to classify the complex fluids, J. Non-Newtonian Fluid Mech. **107**, 51 (2002).
[14] V. Tirtaatmadja and T. Sridhar, A filament stretching device for measurement of extensional viscosity, J. Rheol. **37**, 1081 (1993).
[15] G. H. Mckinley and T. Sridhar, Filament-stretching rheometry of complex fluids, Annu. Rev. Fluid Mech. **34**, 375 (2002).
[16] H. K. Rasmussen, P. Laillé, and K. Yu, Large amplitude oscillatory elongation flow, Rheol. Acta **47**, 97 (2008).
[17] A. G. Bejenariu, H. K. Rasmussen, A. L. Skov, O. Hassager, and S. M. Frankaer, Large amplitude oscillatory extension of soft polymeric networks, Rheol. Acta **49**, 807 (2010).
[18] S. J. Haward, V. Sharma, and J. A. Odell, Extensional opto-rheometry with biofluids and ultra-dilute polymer solutions, Soft Matter **7**, 9908 (2011).
[19] E. S. G. Shaqfeh, The dynamics of single-molecule DNA in flow, J. Non-Newtonian Fluid Mech. **130**, 1 (2005).
[20] D. J. Mai, C. Brockman, and C. M. Schroeder, Microfluidic systems for single DNA dynamics, Soft matter **8**, 10560 (2012).
[21] T. T. Perkins, D. E. Smith, R. G. Larson, and S. Chu, Stretching of a single tethered polymer in a uniform flow, Science (New York) **268**, 83 (1995).
[22] D. E. Smith, H. P. Babcock, and S. Chu, Single-polymer dynamics in steady shear flow, Science (New York) **283**, 1724 (1999).
[23] J. S. Hur, E. S. G. Shaqfeh, H. P. Babcock, D. E. Smith, and S. Chu, Dynamics of dilute and semidilute DNA solutions in the start-up of shear flow, J. Rheol. **45**, 421 (2001).
[24] C. M. Schroeder, R. E. Teixeira, E. S. G. Shaqfeh, and S. Chu, Dynamics of DNA in the flow-gradient plane of steady shear flow: Observations and simulations, Macromolecules **38**, 1967 (2005).
[25] C. M. Schroeder, R. E. Teixeira, E. S. G. Shaqfeh, and S. Chu, Characteristic Periodic Motion of Polymers in Shear Flow, Phys. Rev. Lett. **95**, 018301 (2005).
[26] R. E. Teixeira, H. P. Babcock, E. S. G. Shaqfeh, and S. Chu, Shear thinning and tumbling dynamics of single polymers in the flow-gradient plane, Macromolecules **38**, 581 (2005).
[27] T. T. Perkins, D. E. Smith, and S. Chu, Single polymer dynamics in an elongational flow, Science (New York) **276**, 2016 (1997).
[28] D. E. Smith and S. Chu, Response of flexible polymers to a sudden elongational flow, Science (New York) **281**, 1335 (1998).
[29] C. M. Schroeder, H. P. Babcock, E. S. G. Shaqfeh, and S. Chu, Observation of polymer conformation hysteresis in extensional flow, Science (New York) **301**, 1515 (2003).
[30] C. M. Schroeder, E. S. G. Shaqfeh, and S. Chu, Effect of hydrodynamic interactions on DNA dynamics in extensional flow: Simulation and single molecule experiment, Macromolecules **37**, 9242 (2004).
[31] J. S. Hur, E. S. G. Shaqfeh, H. P. Babcock, and S. Chu, Dynamics and configurational fluctuations of single DNA molecules in linear mixed flows, Phys. Rev. E **66**, 011915 (2002).
[32] H. P. Babcock, R. E. Teixeira, J. S. Hur, E. S. G. Shaqfeh, and S. Chu, Visualization of molecular fluctuations near the critical point of the coil-stretch transition in polymer elongation, Macromolecules **36**, 4544 (2003).
[33] P. G. de Gennes, Molecular individualism, Science (New York) **276**, 1999 (1997).
[34] A. Shenoy, C. V. Rao, and C. M. Schroeder, Stokes trap for multiplexed particle manipulation and assembly using fluidics, Proc. Natl. Acad. Sci. USA **113**, 3976 (2016).
[35] A. Groisman, M. Enzelberger, and S. R. Quake, Microfluidic memory and control devices, Science (New York) **300**, 955 (2003).
[36] M. Tanyeri, M. Ranka, N. Sittipolkul, and C. M. Schroeder, A microfluidic-based hydrodynamic trap: Design and implementation, Lab. Chip **11**, 1786 (2011).
[37] D. E. Smith, T. T. Perkins, and S. Chu, Dynamical scaling of DNA diffusion coefficients, Macromolecules **29**, 1372 (1996).
[38] B. Kundukad, J. Yan, and P. S. Doyle, Effect of YOYO-1 on the mechanical properties of DNA, Soft Matter **10**, 9721 (2014).

[39] R. C. H. Van Der Burgt, P. D. Anderson, J. M. J. D. Toonder, and F. N. Van De Vosse, A microscale pulsatile flow device for dynamic cross-slot rheometry, Sensors Actuators A **220**, 221 (2014).
[40] T. T. Perkins, S. R. Quake, D. E. Smith, and S. Chu, Relaxation of a single DNA molecule observed by optical microscopy, Science (New York) **264**, 822 (1994).
[41] R. M. Jendrejack, J. J. De Pablo, and M. D. Graham, Stochastic simulations of DNA in flow: Dynamics and the effects of hydrodynamic interactions, J. Chem. Phys. **116**, 7752 (2002).
[42] H. C. Öttinger, *Stochastic Processes in Polymeric Fluids* (Springer-Verlag, Berlin, Germany, 1996).
[43] J. Rotne and S. Prager, Variational treatment of hydrodynamic interaction in polymers, J. Chem. Phys. **50**, 4831 (1969).
[44] M. Somasi, B. Khomami, N. J. Woo, J. S. Hur, and E. S. G. Shaqfeh, Brownian dynamics simulations of bead-rod and bead-spring chains: Numerical algorithms and coarse-graining issues, J. Non-Newtonian Fluid Mech. **108**, 227 (2002).
[45] J. F. Marko and E. D. Siggia, Stretching DNA, Macromolecules **28**, 8759 (1995).
[46] J. R. Prakash, Rouse chains with excluded volume interactions in steady simple shear flow, J. Rheol. **46**, 1353 (2002).
[47] C.-C. Hsieh, L. Li, and R. G. Larson, Modeling hydrodynamic interaction in Brownian dynamics: Simulations of extensional flows of dilute solutions of DNA and polystyrene, J. Non-Newtonian Fluid Mech. **113**, 147 (2003).
[48] R. G. Larson, The role of molecular folds and "pre-conditioning" in the unraveling of polymer molecules during extensional flow, J. Non-Newtonian Fluid Mech. **94**, 37 (2000).
[49] G. G. Fuller and L. G. Leal, The effects of conformation-dependent friction and internal viscosity on the dynamics of the nonlinear dumbbell model for a dilute polymer solution, J. Non-Newtonian Fluid Mech. **8**, 271 (1981).
[50] R. G. Larson and J. J. Magda, Coil-stretch transitions in mixed shear and extensional flows of dilute polymer solutions, Macromolecules **22**, 3004 (1989).
[51] W. H. Press, S. A. Teukolsky, W. T. Vetterling, and B. P. Flannery, *Numerical Recipes: The Art of Scientific Computing*, 3rd ed. (Cambridge University Press, New York, 2007).
[52] A. C. Pipkin, *Lectures on Viscoelasticity Theory* (Springer-Verlag, New York, 1972).
[53] D. J. Mai, A. B. Marciel, C. E. Sing, and C. M. Schroeder, Topology-controlled relaxation dynamics of single branched polymers, ACS Macro Lett. **4**, 446 (2015).
[54] Y. Li, K.-W. Hsiao, C. A. Brockman, D. Y. Yates, R. M. Robertson-Anderson, J. A. Kornfield, M. J. San Francisco, C. M. Schroeder, and G. B. McKenna, When ends meet: Circular DNA stretches differently in elongational flows, Macromolecules **48**, 5997 (2015).